Supplement of Atmos. Chem. Phys., 24, 11943–11954, 2024
https://doi.org/10.5194/acp-24-11943-2024-supplement

Atmospheric Chemistry and Physics Open Access

Supplement of

Formation of reactive nitrogen species promoted by iron ions through the photochemistry of a neonicotinoid insecticide

Zhu Ran et al.

Correspondence to: Yanan Hu (huyanan0917@163.com), Sasho Gligorovski (gligorovski@gig.ac.cn), and Jiangping Liu (liujiangping18@mails.ucas.ac.cn)

Supplementary Text

Text S1. Ionic analysis at different Fe^{3+} concentrations

As depicted in Figure S5, the direct photolysis of NPM produced a large amount of NO_3^- and NO_2^- in the absence of Fe^{3+}, and in the presence of Fe^{3+} restricted NO_3^- and NO_2^- production occurred, which was consistent with the change of the photolysis rate constant of NPM. NO_2 produced by direct photolysis of NPM is hydrolyzed in aqueous media to form NO_2^- and NO_3^-, and nitrogenous species are partially dissolved during their release from the liquid to the gas phase. The reaction of NOx with $O_2^{-\bullet}$ radicals will also produce NO_2^- and NO_3^-. The presence of Fe^{3+} provides a strong acid environment (Table S1) and the protonation of NO_2^- will lead to the release of HONO (Lu et al., 2015; Wang et al., 2021). Upon irradiation at λ>300 nm, Fe^{3+} species (monomeric and dimeric) are known to undergo a redox process giving rise to Fe(II) and •OH radicals (Bai et al., 2023). Fe^{2+} cannot coexist with NO_3^-, and NO_2 gas will be produced by redox reaction. In short, the addition of Fe^{3+} promotes the conversion of NO_3^- and NO_2^- to HONO and NOx. In the presence of high Fe^{3+} concentration, the photolysis rate of NPM showed an increasing trend, and •OH and $O_2^{-\bullet}$ produced under light irradiation were more elevated than those produced under low concentration of Fe^{3+} (Figure 4), which slightly promoted the generation of NO_3^- and NO_2^-.

Text S2. Global simulation of NOx and HONO fluxes

We are estimating the amount of NOx and HONO fluxes released from NPM chemistry, as a function of NPM concentration and solar radiation, following Eq-S1, Eq-S2 and Eq-S3, but assuming that the environmental NPM concentration is three orders smaller (50 μg L^{-1}) than the experimental conditions of 50000 μg L^{-1}. The parameterization of HONO and NOx productions from NPM photolysis at Fe^{3+} concentration of 0.025 mg L^{-1} used in our estimation is based on Eq-S1, Eq-S2 and Eq-S3 (Figure S8 and Figure S9). The estimation is conducted for each of the 561×360 grids at the globe with a horizontal resolution of 0.5×0.625°, consistent with resolution of the solar radiation data from the hourly Modern-Era Retrospective analysis for Research and Applications Version 2 (MERRA2) reanalysis dataset.

Y_{HONO}=1.58595*10^9X-1.19123*10^11 Eq-S1

Y_{NO2}=6.58261*10^8X-1.81889*10^10 Eq-S2

Y_{NO}=2.58054*10^8X-1.41507*10^10 Eq-S3

Where Y(molecules cm^{-2} s^{-1}) represents the HONO/NOx fluxes, X (W m^{-2}) represents the light density. A key procedure is to consider the concentration of NPM at each of the 0.5×0.625°grids. Ideally, the NPM concentration should display spatial distributions as the iron contents, solar light intensity and underlying surface is different for each region.

We have to stress that our experiment is not able to derive the relationship between HONO, NOx emissions and light density at NPM concentration lower than 50000 μg L^{-1} due to the current limit of detection. As such, we assume that the environmental NPM concentration is three orders smaller (50 μg L^{-1}) than the experimental conditions of 50000 μg L^{-1}, and do not consider its spatial heteorogenity in the model. As a result, the variation of NOx and HONO emissions is driven by the solar radiation. We summarized the distribution of soluble iron concentrations in the waters as shown in Table S3 in the supplementary information. In order to estimate the environmental NPM and iron concentration contributed to the formation of reactive nitrogen species, we selected a rationalization parameter scheme related to the environmental concentration of NPM (50 μg L^{-1}) and soluble iron (92.48 nmol L^{-1}, 0.025 mg L^{-1} in our study), which is representative of certain significance.

Furthermore, the widespread use of NPM and its capability to release HONO and NOx suggests that NPM might be an unexplored source of global atmospheric reactive nitrogen (Nr) and hence influence air quality and climate. Evaluation of such impacts requires a parameterization of global HONO and NOx fluxes emerging from NPM photochemistry in chemical transport models. However, current chemical models do not explicitly consider this source of reactive nitrogen species. In this manner, we are able to generate an hourly dataset of the NOx and HONO fluxes released from NPM chemistry, and we analyze the amount and spatial pattern of the fluxes in Figure 5. We note that although such estimation is rather simplified and can be biased in terms of the spatial heterogeneity as we do not consider the spatial variation of environmental NPM concentrations, our study presents a pioneer attempt to quantify the global source of HONO and NOx from the NPM photochemistry, as current chemical models do not explicitly consider this source of reactive nitrogen species. This inventory can be then applied in chemical models to quantify the environmental impact of HONO and NOx fluxes emerging from NPM photochemistry.

Text S3. Calculation of Quantum Yields

The quantum yields for reactive nitrogen species formation (Φ), including Φ_{HONO} and Φ_{NOx} can be determined by the equation (Eq-S4 and Eq-S5).

$$\emptyset_{HONO} = \frac{J_{NPM \rightarrow HONO}}{\int_{\lambda_1}^{\lambda_2} I(\lambda)\,\sigma(\lambda)\,d\lambda} \qquad \text{Eq-S4}$$

$$\emptyset_{NOx} = \frac{J_{NPM \rightarrow NOx}}{\int_{\lambda_1}^{\lambda_2} I(\lambda)\,\sigma(\lambda)\,d\lambda} \qquad \text{Eq-S5}$$

Where I(λ) (photons cm^{-2} s^{-1}) and σ(λ) (cm^2 $molecules^{-1}$) are the actinic flux spectra of light source and the absorption cross section of the NPM, respectively (Figure S10).

Table S1. Measured Photolysis Rate Constants (k) and Half-time ($T_{1/2}$) of NPM in aqueous solution at different Fe^{3+} concentrations.

The concentration of Fe^{3+} ($mg.ml^{-1}$)	Kinetic equation	Rate Constants (k)/min^{-1}	Half-time ($T_{1/2}$)/min	R^2	Initial pH value
0	$C_t = 0.501e^{-0.00427t}$	0.00427	162.3	0.99438	7.3
0.1	$C_t = 0.477e^{-0.00382t}$	0.00382	181.5	0.98757	3.4
0.25	$C_t = 0.520e^{-0.00310t}$	0.00310	223.6	0.98065	2.9
0.5	$C_t = 0.514e^{-0.00346t}$	0.00346	200.3	0.98869	2.6
0.8	$C_t = 0.513e^{-0.00513t}$	0.00513	135.1	0.99064	2.4

Table S2. Quantum Yields (ϕ) for Photolysis of NPM and NOx at different Fe^{3+} concentrations

The concentration of Fe^{3+} (mg ml^{-1})	**0**	**0.1**	**0.25**	**0.5**	**0.8**
ϕ_{HONO}	4.48×10^{-5}	1.84×10^{-4}	2.03×10^{-4}	1.59×10^{-4}	1.55×10^{-4}
ϕ_{NO2}	2.03×10^{-5}	6.46×10^{-5}	5.21×10^{-5}	4.71×10^{-5}	4.02×10^{-5}
ϕ_{NO}	4.06×10^{-5}	3.35×10^{-5}	2.10×10^{-5}	1.87×10^{-5}	1.40×10^{-5}

Table S3. The concentrations of soluble iron in water of different region

Sampling site	Concentration (nmol L^{-1})	References
Humic acid-rich coast of the Pacific Ocean	23.1-573.2	Gerringa et al., 2007
Scheldt estuary	104-536	Batchelli et al., 2010
Peconic Estuary	9-240	Gobler et al., 2002
Southern Vancouver Island	0.05 – 0.07	Nishioka et al., 2001
Alaskan coastal waters	0.5-4.1	Lippiatt et al., 2010
the outer bay of Mediterranean coastal waters	3.7-25	Öztürk et al., 2003
in the inner and middle bay of Mediterranean coastal waters	9-240	
Yamuna River in Mathura	1.73 mg L^{-1}	Ahmed et al., 2022

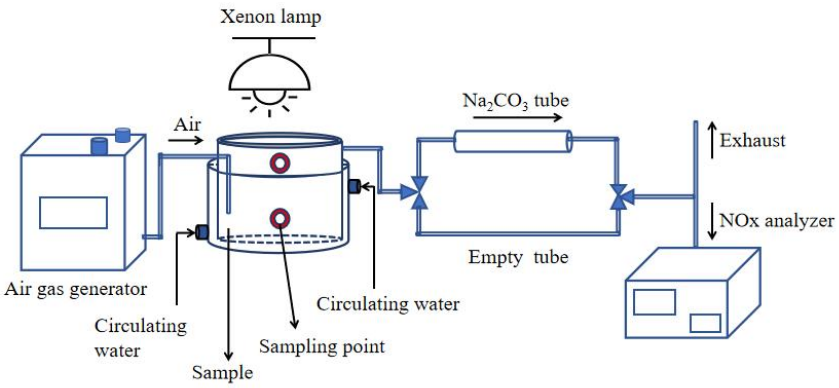

104

105 **Figure S1.** Diagram of the experimental set up

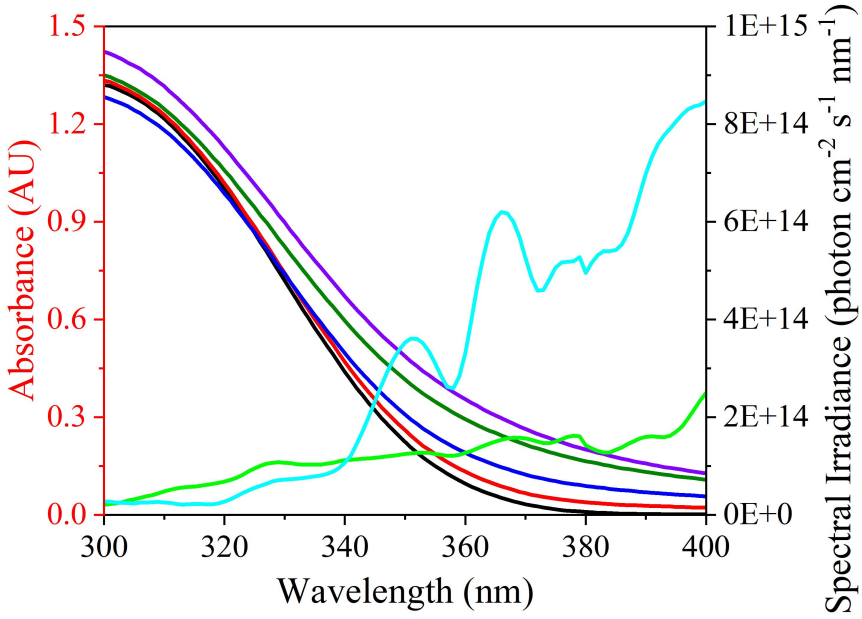

Figure S2. The absorption spectra of NPM (0.05 mg ml^{-1}) in the absence of Fe^{3+} (dark line), and in the presence of different concentrations of Fe^{3+}: 0.01 mg ml^{-1} (red line), 0.025 mg ml^{-1} (blue line), 0.05 mg ml^{-1} (green line) and 0.08 mg ml^{-1} (purple line). Comparison of the spectral irradiance of the Xenon lamp (Fluorescent light blueed line) and the spectral irradiance of the sunlight (fluorescent light green line) measured by the spectroradiometer (HP350UVP, China). The spectral irradiance is determined for Kunming (latitude 24.85285, longitude 102.86016) on July 26 2022 at noon.

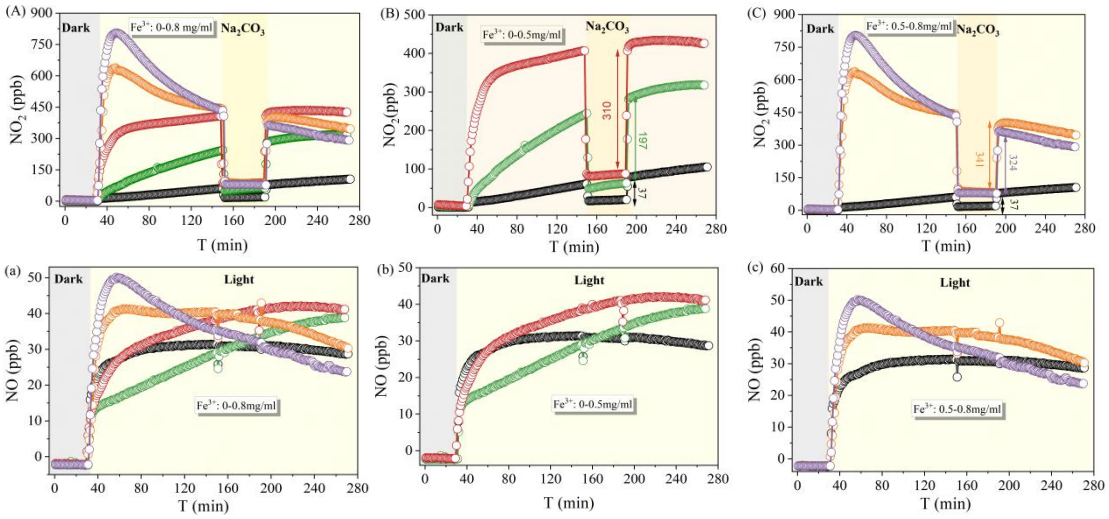

Figure S3. The temporal changes of NO_2, HONO and NO during the photolysis of NPM (0.5 mg ml^{-1}) in the absence of Fe^{3+} (dark line), and in the presence of different concentrations of Fe^{3+}: 0.1 mg ml^{-1} (blue line), 0.25 mg ml^{-1} (red line), 0.5 mg ml^{-1} (orange line) and 0.8 mg ml^{-1} (purple line). Reaction conditions: irradiation intensity of 169.4 W m^{-2} at 300-400 nm, temperature of 298 K.

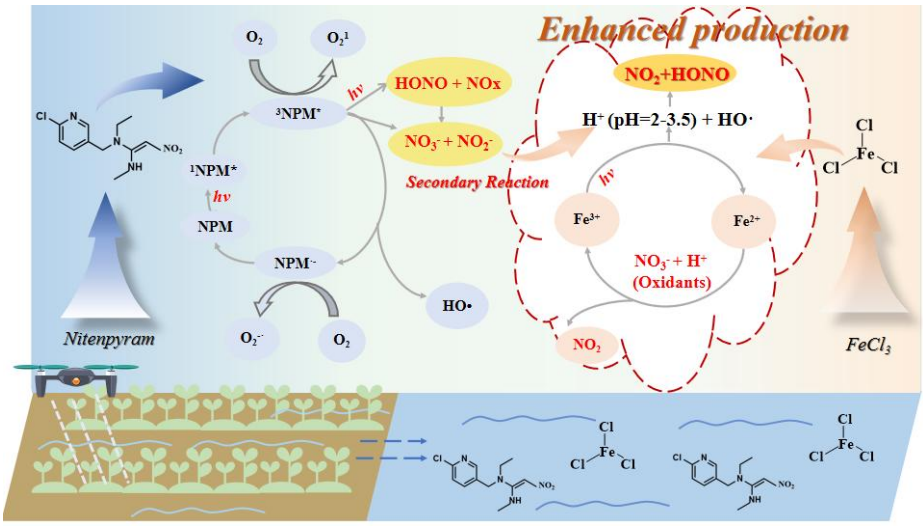

121

122 **Figure S4.** Proposed mechanism of NPM photolysis in the presence of iron ions leading to HONO and NOx
123 formation.

124

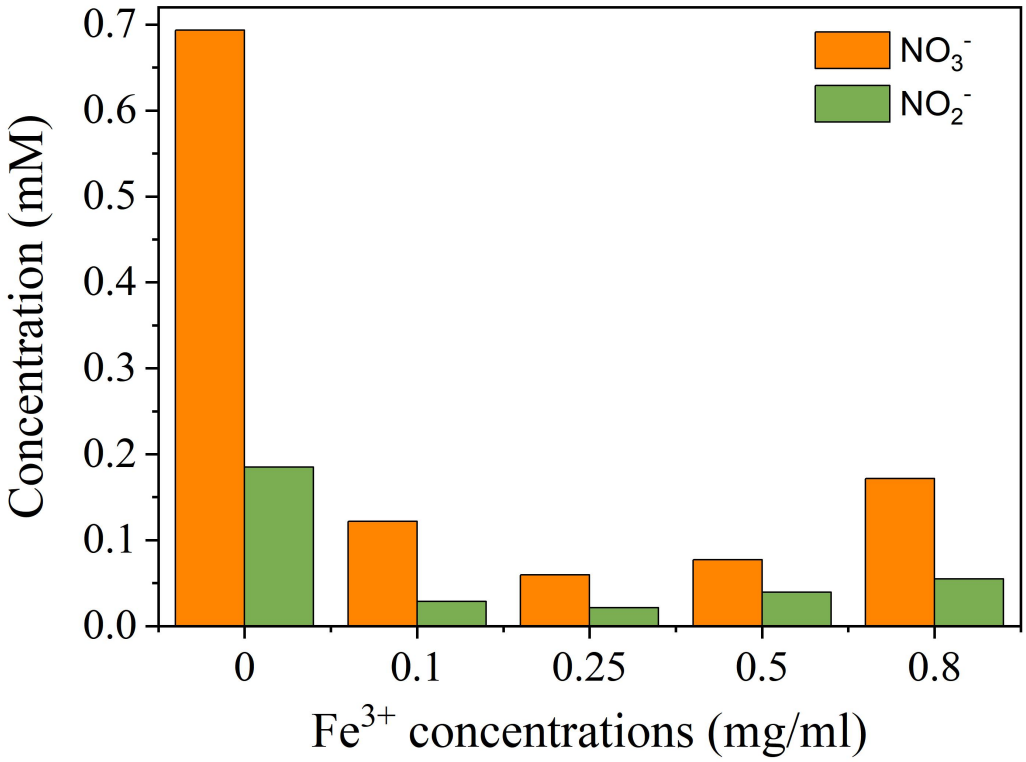

125

126

127 **Figure S5.** The nitrate and nitrite ions concentrations of NPM (0.5 mg ml^{-1}) by 2 hours photolysis at different
128 concentrations of Fe^{3+}.

129

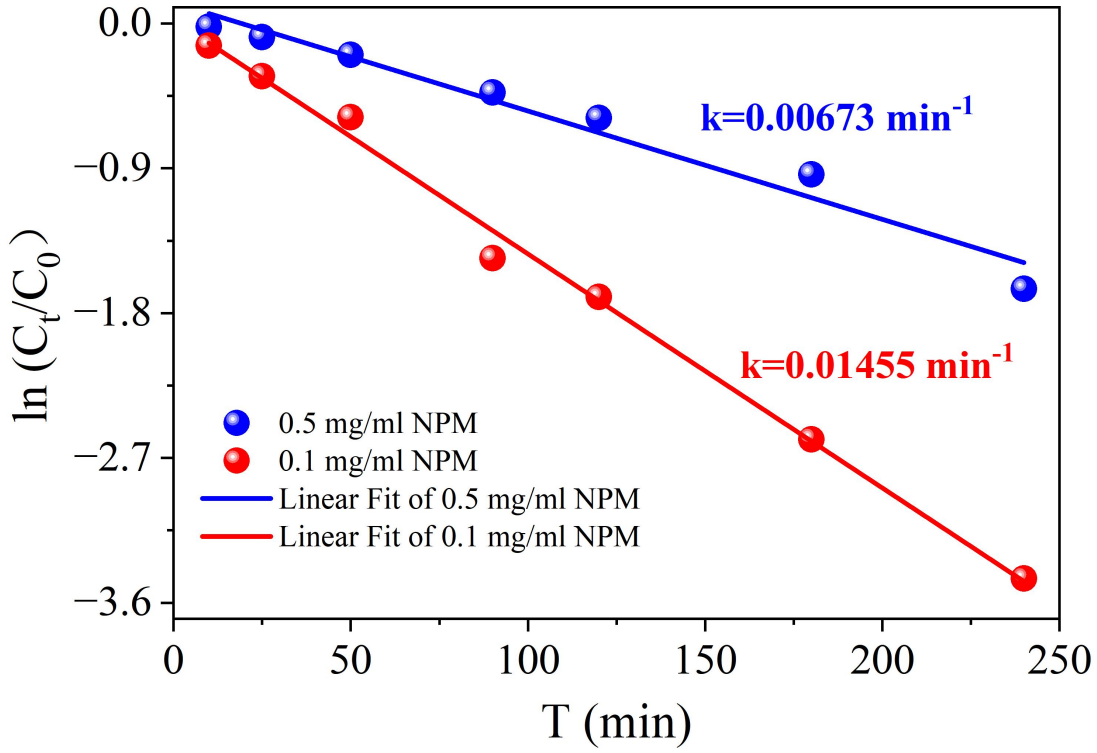

130

131 **Figure S6.** First-order rates at different NPM concentrations

132

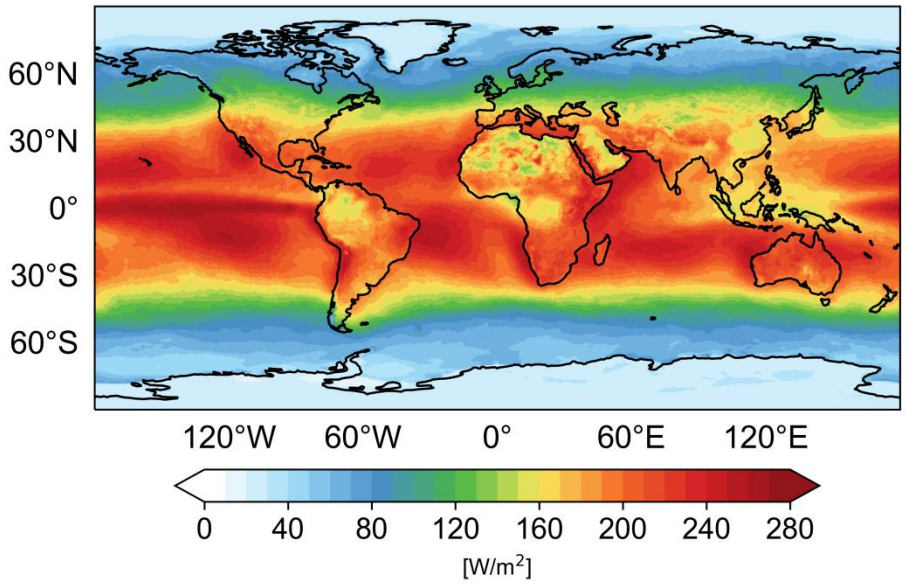

Figure S7. The spatial distribution of solar radiation in the global region.

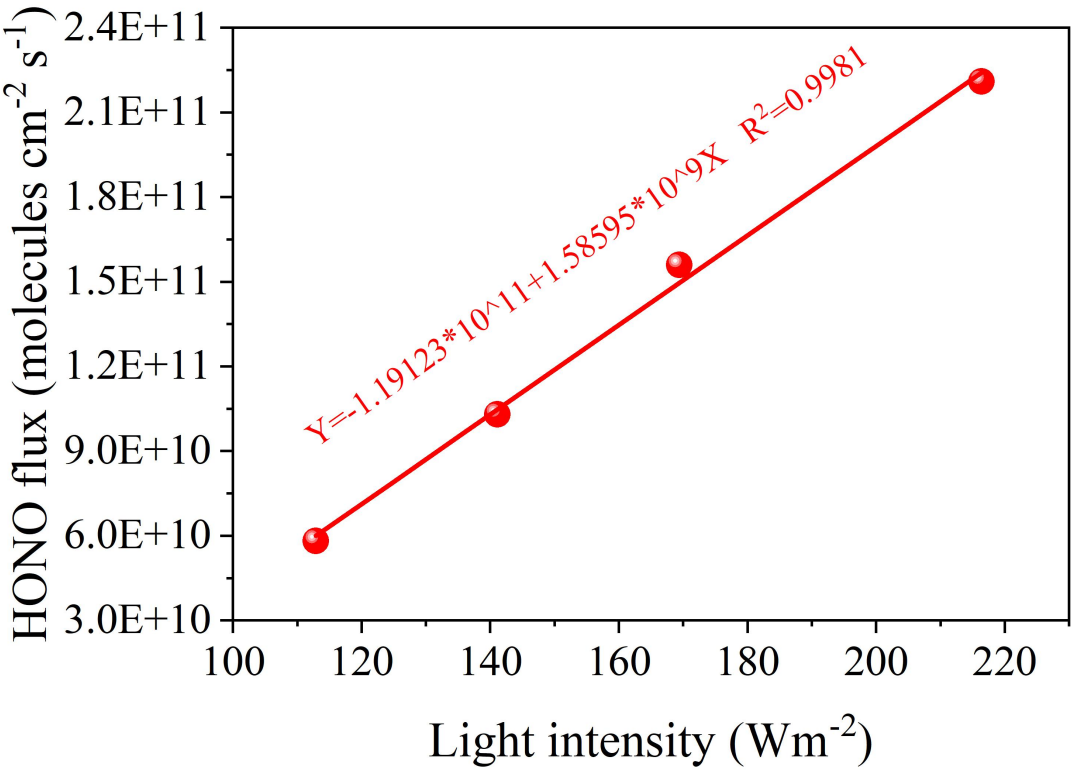

135

136

137 **Figure S8.** HONO flux from NPM photolysis under different light intensity. Conditions: NPM concentration of

138 0.05 mg ml^{-1}, Fe^{3+} concentration of 0.025 mg ml^{-1}, irradiation time of 60 min, temperature of 298 K.

139

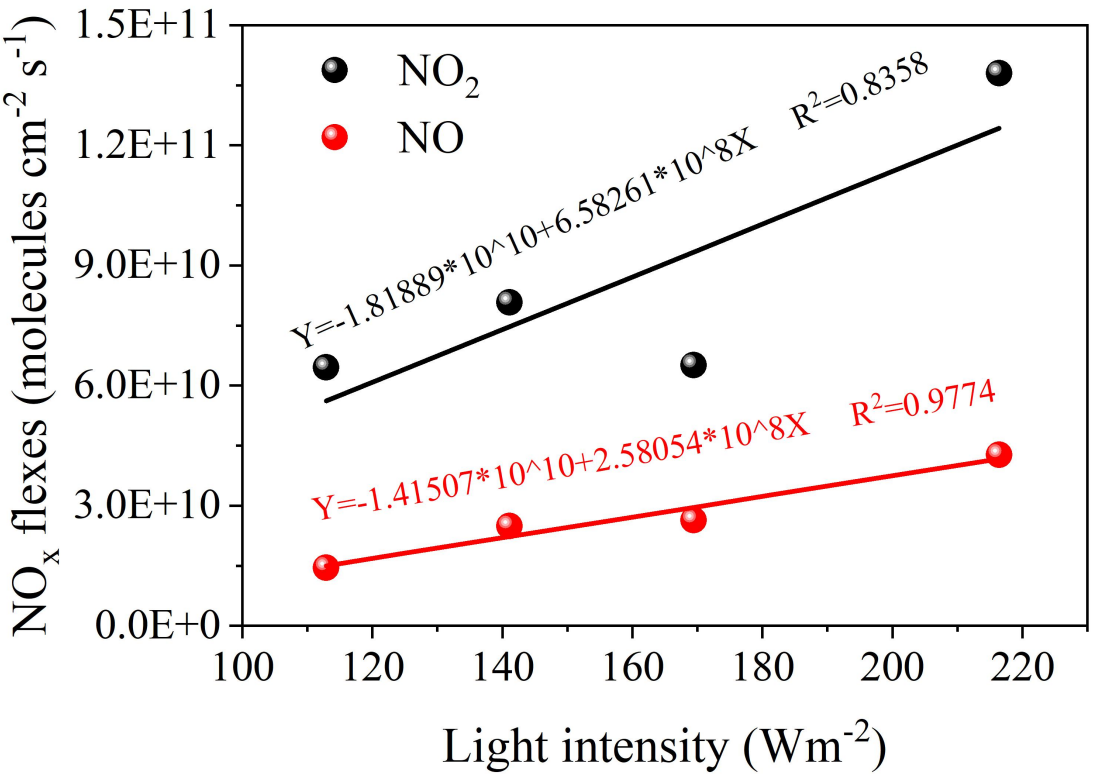

140

141

142 **Figure S9.** NOx flux from NPM photolysis under different light intensity. Conditions: NPM concentration of 0.05
143 mg ml^{-1}, Fe^{3+} concentration of 0.025 mg ml^{-1}, irradiation time of 60 min, temperature of 298 K.

144

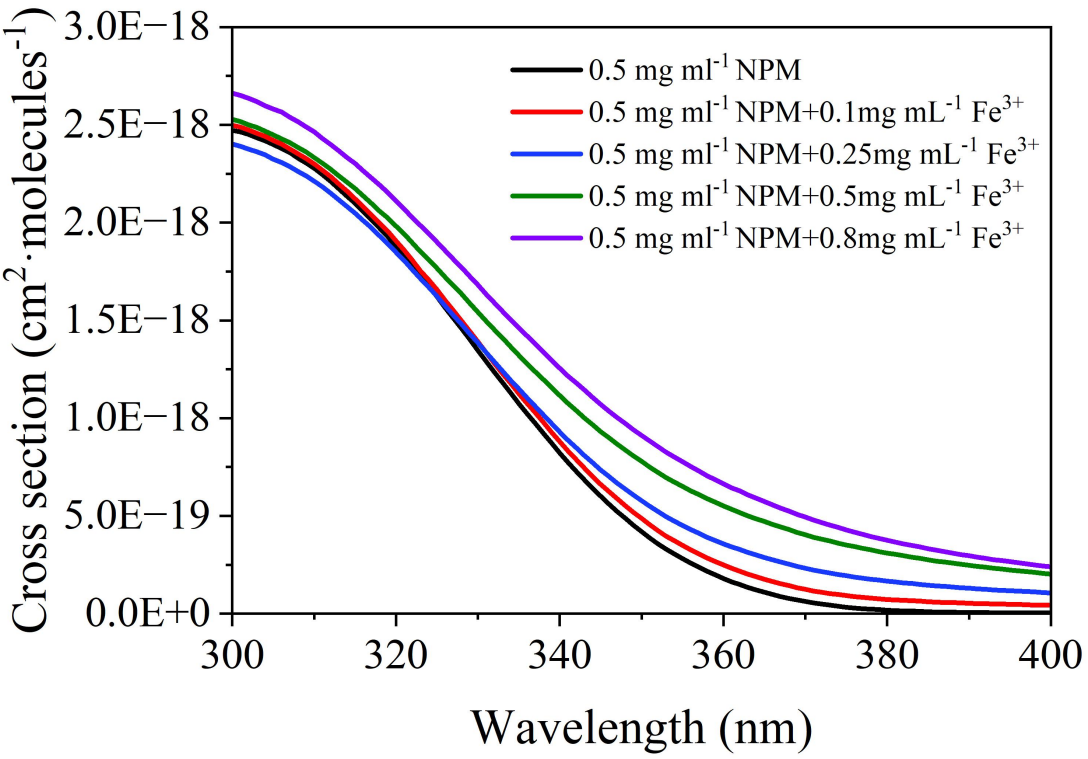

145

Figure S10. Cross section of NPM and NOx at different Fe^{3+} concentrations.

References

Ahmed, S., Akhtar, N., Rahman, A., Mondal, N. C., Khurshid, S., Sarah, S., Muqtada Ali Khan, M., and Kamboj, V.: Evaluating groundwater pollution with emphasizing heavy metal hotspots in an urbanized alluvium watershed of Yamuna River, northern India, Environ. Nanotechnol., Monit. Manage, 18, 10744, doi:10.1016/j.enmm.2022.100744, 2022.

Bai, X., Yang, Q., Guo, Y., Hao, B., Zhang, R., Duan, R., and Li, J.: Alkyl halide formation from degradation of carboxylic acids in the presence of Fe(III) and halides under light irradiation, Water. Res., 235, 119842, doi:10.1016/j.watres.2023.119842, 2023.

Batchelli, S., Muller, F. L. L., Chang, K.-C., and Lee, C.-L.: Evidence for Strong but Dynamic Iron−Humic Colloidal Associations in Humic-Rich Coastal Waters, Environ. Sci. Technol., 44, 8485-8490, doi:10.1021/es101081c, 2010.

Gerringa, L. J. A., Rijkenberg, M. J. A., Wolterbeek, H. T., Verburg, T. G., Boye, M., and de Baar, H. J. W.: Kinetic study reveals weak Fe-binding ligand, which affects the solubility of Fe in the Scheldt estuary, Mar. Chem., 103, 30-45, doi:10.1016/j.marchem.2006.06.002, 2007.

Gobler, C. J., Donat, J. R., Consolvo, J. A.and Sañudo-Wilhelmy, S. A.: Physicochemical speciation of iron during coastal algal blooms, Mar. Chem., 77, 71-89, doi:Doi 10.1016/S0304-4203(01)00076-7, 2002.

Lippiatt, S. M., Lohan, M. C., and Bruland, K. W.: The distribution of reactive iron in northern Gulf of Alaska coastal waters, Mar. Chem., 121, 187-199, doi:10.1016/j.marchem.2010.04.007, 2010.

Lu, Z., Challis, J. K., and Wong, C. S.: Quantum Yields for Direct Photolysis of Neonicotinoid Insecticides in Water: Implications for Exposure to Nontarget Aquatic Organisms, Environ. Sci. Technol. Lett., 2, 188-192, doi:10.1021/acs.estlett.5b00136, 2015.

Nishioka, J., Takeda, S., Wong, C. S., and Johnson, W. K.: Size-fractionated iron concentrations in the northeast Pacific Ocean: distribution of soluble and small colloidal iron, Mar. Chem., 74, 157-179, doi:Doi 10.1016/S0304-4203(01)00013-5, 2001.

Öztürk, M., Bizsel, N., and Steinnes, E.: Iron speciation in eutrophic and oligotrophic Mediterranean coastal waters;: impact of phytoplankton and protozoan blooms on iron distribution, Mar. Chem., 81, 19-36, doi:10.1016/S0304-4203(02)00137-8, 2003.

Wang, Y., Huang, D. D., Huang, W., Liu, B., Chen, Q., Huang, R., Gen, M., Mabato, B. R. G., Chan, C. K., Li, X., Hao, T., Tan, Y., Hoi, K. I., Mok, K. M., and Li, Y. J.: Enhanced Nitrite Production from the Aqueous Photolysis of Nitrate in the Presence of Vanillic Acid and Implications for the Roles of Light-Absorbing Organics, Environ. Sci. Technol. Lett., 55, 15694-15704, doi:10.1021/acs.est.1c04642, 2021.